Chapter

Microwave Heating of Liquid Crystals and Ethanol-Hexane Mixed Solution and Its Features (Review)

Akira Naito, Yugo Tasei, Batsaikhan Mijiddorj, Izuru Kawamura and Kazuyoshi Ueda

Abstract

Microwave heating is widely used to accelerate organic reactions in the chemistry field. However, the effect of microwaves on chemical reaction has not yet been well characterized at the molecular level. In this review chapter, microwave heating processes of liquid crystals and an ethanol-hexane mixed solution under microwave irradiation were experimentally and theoretically investigated using *in situ* microwave irradiation nuclear magnetic resonance (NMR) spectroscopy and molecular dynamics (MD) simulation, respectively. The temperature of the solution under microwave irradiation was estimated from a chemical shift calibrated temperature (CSC-temperature) which was determined from the temperature dependence of the ^{1}H chemical shift. The CSC-temperatures of CH_2 and CH_3 non-polar protons of ethanol reflect the bulk temperature of a solution by the thermal microwave effect. The lower CSC-temperature of the OH polar protons in ethanol and much higher CSC-temperature of H-C=N (7′) and CH_3-O (α') protons of N-(4-methoxybenzyliden)-4-butylaniline with respect to the bulk temperature are attributed to the non-thermal microwave effects. According to the MD simulation under microwave irradiation, the number of hydrogen bonds increased in the ethanol-hexane mixed solution as a result of a non-thermal microwave effect. It is concluded that a coherently ordered low entropy state of polar molecules is induced by a non-thermal microwave effect. The ordered state induces molecular interaction, which may accelerate the chemical reaction rate between molecules with polar groups.

Keywords: microwave heating mechanism, microwave irradiation NMR spectroscopy, MD simulation, thermal microwave effect, non-thermal microwave effect

1. Introduction

Microwave heating effects in the field of chemical science are attributed to an increase in the solvent temperature due to dielectric loss [1–6]. Dipole moments of the solvent molecules align along an applied electric field that oscillates in the case of microwaves. As the dipoles attempt to align along this alternating electric field, which is a low entropy state, heat energy is produced by molecular friction

and collision, which increases entropy and the energy is dissipated through the system. From a thermodynamic point of view, this microwave energy converts to heat energy (thermal effect) and work energy such as volume change (non-thermal effect). However, the detailed molecular mechanisms associated with thermal and non-thermal microwave effects on the chemical reaction rates have not yet been fully elucidated. In particular, the non-thermal microwave effect has not yet been well characterized [7]. In the field of chemistry, microwave heating is widely used to accelerate organic synthesis reactions [2–4, 7–14], reduce polymerization reaction times [15–18], and enhance the activity of enzymes in the field of biological chemistry [19–21]. The majority of accelerated reactions achieved in this manner can be mainly explained by the thermal microwave effect [7, 22]. Non-thermal microwave effects have also been identified and the thermal and non-thermal microwave effects can be distinguished [23]. The non-thermal microwave effects have recently been demonstrated by the observation of an increasing polymerization reaction rate under microwave electric fields and a decrease in the rates under microwave magnetic fields [18]. Nevertheless, non-thermal microwave effects at the molecular level are still controversial [7]. In particular, non-thermal microwave effects have been considered as a direct interaction of the electric field with polar molecules in the reaction medium which is not explained with a macroscopic temperature effect [2, 22]. The presence of an electric field leads to effects on the orientation of dipolar molecules or intermediates, and thus changes the pre-exponential factor A or the activation energy in the Arrhenius equation for certain types of reactions [2, 22].

As a specific microwave heating effect, non-equilibrium localized heating is defined as the generation of isolated regions with a much higher temperature than the bulk solution. This has been observed in liquid–solid systems under microwave irradiation, such as in the case of dimethyl sulfoxide (DMSO) molecules in contact with Co particles under microwave irradiation [24].

To characterize the microwave heating mechanism with the molecular resolution, microwave-irradiation nuclear magnetic resonance (NMR) spectroscopy was first developed by Naito et al. [25]. The characteristic that microwave heating causes a rapid temperature jump was used to obtain state-correlated two-dimensional (2D) NMR spectra between liquid crystalline and isotropic phases. This enabled high-resolution observation of a ^{1}H-^{1}H dipolar pattern in the cross section of the ^{1}H state-correlated 2D NMR spectra of the liquid state toward the liquid crystalline state. The local dipolar interaction of individual protons in the liquid crystalline state can be examined via high-resolution resonance in the isotropic phase [26–30]. The resulting data can also be used to obtain state-correlated 2D NMR spectra of proteins in the native and denatured states [31].

In situ microwave irradiation NMR spectroscopy was developed later [32], and the microwave heating process was observed in liquid crystalline samples [32, 33] and ethanol-hexane mixed solution [34]. The *in situ* temperature of the bulk solution was determined using the relation between ^{1}H chemical shift and temperature. This temperature is defined as chemical shift calibrated temperature (CSC-temperature) and is measured for individual protons. In N-(4-methoxybenzylidene)-4-butylaniline (MBBA) molecules, H-C=N (7′), and CH_3-O (α') protons showed significantly higher CSC-temperatures than the bulk temperature in the isotropic state [33]. In the ethanol-hexane mixed solution, OH proton showed lower CSC-temperature than that of the bulk solution [34].

Molecular dynamics (MD) simulations have recently been conducted to investigate the atomic-scale properties of molecular systems under an electric field. Tanaka and Sato investigated the heating process of water and ice under microwave irradiation. They observed that the rotational motion of the water was delayed due to the microwave electric field, and the energy is transferred to the kinetic and

intermolecular energies of water [5]. Caleman and van der Spoel described that an infrared (IR) laser pulse energy rapidly increased the intramolecular bond vibrations, and the energy was transferred to rotational and translational motion of ice using MD simulations [35]. Marklund et al. investigated the different orientations of a protein depending on the range of electric field strengths without loss of the structure [36]. English and MacElroy conducted MD simulations and found that microwave heating was more efficient for polarizable water models than for non-polarizable models. [37, 38].

This chapter describes the microwave heating processes for common organic solvents, a mixed solution of ethanol (polar molecule) and hexane (non-polar molecule), and liquid crystalline and isotropic phases of MBBA systems. CSC-temperature was employed to accurately measure the temperature of the bulk solution during microwave irradiation [39]. In the case of diamagnetic nuclei, it has been reported that the temperature dependence of the chemical shift values is typically linear [40–44]: therefore, the CSC-temperatures of the individual groups of molecules under microwave irradiation were assessed using *in situ* microwave irradiation NMR spectroscopy.

2. *In situ* microwave irradiation NMR spectrometer

The *in situ* microwave NMR spectrometer employed consisted of a solid-state NMR spectrometer and a microwave generator that was capable of transmitting 1.3 kW continuous wave (CW) and pulsed microwaves at a frequency of 2.45 GHz (**Figure 1A**). This spectrometer enables NMR signals to be obtained without the interference of microwaves, while radio waves and microwave irradiation are

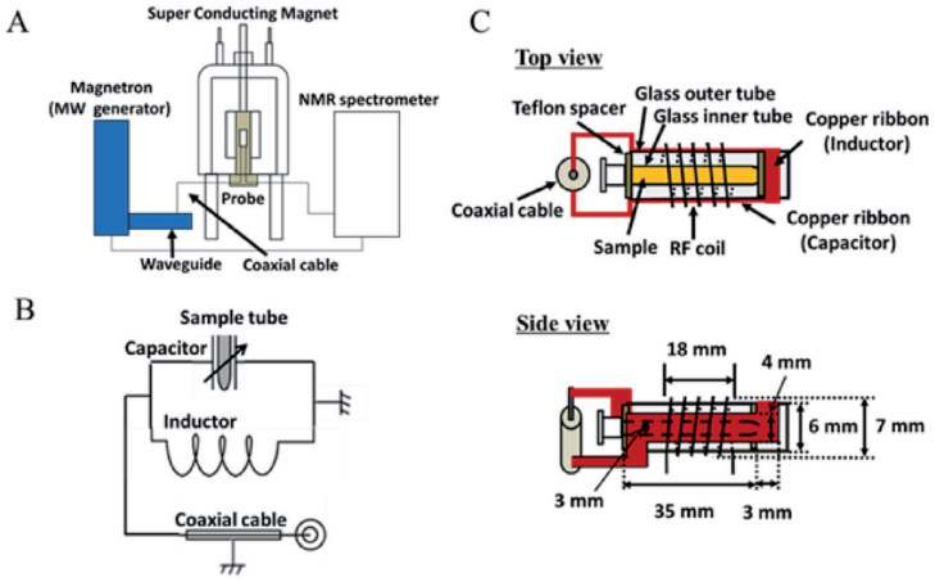

Figure 1.
(A) In situ microwave irradiation solid-state NMR spectrometer which consists of a superconducting magnet, an NMR spectrometer (CMX infinity 400, Chemagnetics), and a microwave transmitter (IDX, 1.3 kW, Tokyo electron Co., ltd.). CW and pulsed microwave are gated by the pulse programmer of the NMR spectrometer. Microwaves are generated and transmitted through a waveguide and coaxial cable, and finally introduced to the microwave resonance circuit in the probe. (B) Equalizing microwave resonance circuit consisting of an inductor and capacitor. The sample tube was located inside the capacitor. (C) Schematic diagrams of microwave resonance and radio wave resonance circuits. The top view indicates the names of components and the side view shows the dimensions of the components. Adapted with permission from [32]. Copyright (2015) Elsevier Inc.

simultaneously applied. Therefore, *in situ* NMR observation is possible under microwave irradiation using this *in situ* microwave irradiation NMR spectrometer. A 3 mm wide flat copper ribbon was used to form the capacitor of the microwave resonance circuit (**Figure 1B**) and was wound coaxially inside the radio wave circuit to increase isolation during microwave irradiation, which reduced interference between microwaves and radio waves (**Figure 1C**) [32]. The microwave resonance circuit was tuned to 2.45 GHz and the radio wave circuit was set to 398 MHz for ^{1}H NMR using a sweep generator. Microwaves were generated from the microwave generator and transmitted through a waveguide and a coaxial cable, and finally, the microwaves were guided to the resonator circuit at the probe head. ^{1}H NMR signals were obtained using 5.0 μs of 90° pulse under microwave irradiation with the *in situ* microwave irradiation NMR spectrometer. The temperature of the sample was varied using the temperature control unit of the spectrometer. Samples were packed in an inner glass tube to insulate them from thermal contact with the outer glass tube. During microwave irradiation, the temperature was controlled at 0°C for the ethanol-hexane mixed solution and at 50°C for MBBA in the isotropic state.

3. MD simulations of ethanol-hexane (1:1) mixed solution and disordered MBBA molecular system

MD simulations of a mixed solution of hexane and ethanol were performed under conditions with and without an oscillating external electric field using Gromacs-2018.7 [45], with the CHARMM36 force field [46]. The CHARMM36 parameter of the MBBA molecule was generated by CHARMM General Force Field (CGenFF) software [47]. Two different systems were applied. The first system consists of 4500 hexane and 4500 ethanol molecules randomly inserted in a cubic box with an edge size of 11.4 nm. The second system includes 904 arbitrarily oriented MBBA molecules in a cubic box with an edge size of 7.5 nm. Periodic boundary conditions were used in all directions, and an oscillating electric field was applied along the x-axis for both systems. An applied electric field with an intensity of 0.5 V/nm and a frequency of 2.45 GHz that served as the microwave heating process [48] was implemented in the simulations. The systems were minimized using steepest descent minimization to reduce steric clashes and were then equilibrated under a constant number of atoms, volume, and temperature (NVT), and under a constant number of atoms, pressure, and temperature (NPT) for each 100-ps MD run. A simulation of the mixture of ethanol and hexane was conducted without the applied electric field for 50 ns. The last snapshot of the simulation was applied as an initial configuration of eight simulations for 5 ns each at different temperatures of 303, 313, 323, and 333 K in the presence and absence of the electric field. In the case of the MBBA system, the initial simulation was performed for 10 ns. The temperature of 293 K (<liquid crystalline to isotropic phase transition temperature (Tc)) and 315 K (>Tc) were then considered with and without the external electric field. The temperature was controlled by a velocity-rescale thermostat [49], and a Parrinello-Rahman barostat provided 1 atm pressure during the simulations [50]. The particle mesh Ewald method [51, 52] and a cutoff of 14 Å were applied for the long-range electrostatic and short-range nonbonded interactions, respectively. The LINCS algorithm was used to constrain all bonds to equilibrium lengths [53]. The time steps of the simulations were 1 and 2 fs for the hexane-ethanol and MBBA systems, respectively. The data were saved at 1 ps intervals. Gromacs tools were used for data analysis; Grace [54] and VMD [55] software were applied for the plots and the structural representations, respectively.

4. *In situ* temperature measurements under microwave irradiation

The *in situ* temperatures of the ethanol-hexane mixed solution and MBBA in the isotropic state under microwave irradiation were assessed with respect to the variation in ^{1}H chemical shifts with temperature for the sample solution located in the NMR probe. **Figure 2** shows the temperature dependence of the ^{1}H NMR signals of OH, CH_2, and CH_3 protons in ethanol (**Figure 2a**) and the CH_2 and CH_3 protons in hexane (**Figure 2b**) that were observed under temperature control with the NMR spectrometer. The ^{1}H chemical shift changes from that at 0°C (Δδ) were plotted as a function of the temperature.

Δδ plotted as a function of temperature was approximately linear within a small temperature range, as observed in methanol and glycol [40]. ^{1}H NMR spectra of individual protons were measured in the same sample at the same position in the probe and the temperature variation was measured under microwave irradiation. The *in situ* temperatures (CSC-temperature) of the individual protons in the sample solution under microwave irradiation were thus evaluated using the temperature variation of the ^{1}H chemical shifts. It is stressed that the *in situ* temperature of the bulk solution was accurately determined with the CSC-temperature for individual non-polar proton groups under microwave irradiation.

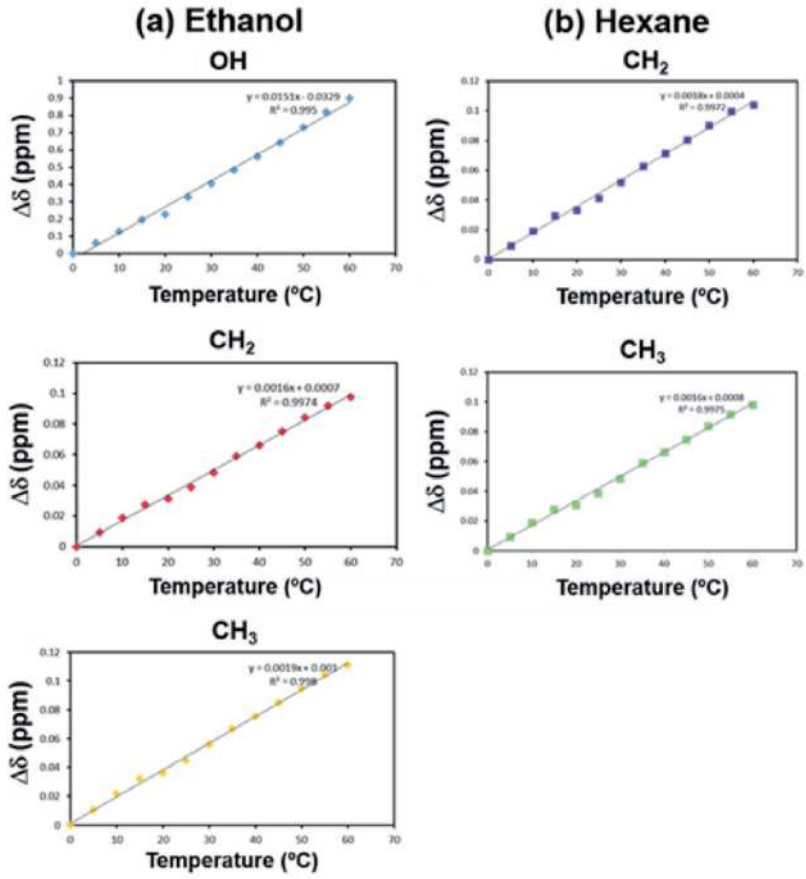

Figure 2.
^{1}H chemical shift changes from ^{1}H chemical shift at 0°C (Δδ) for (a) ethanol OH, CH_2, and CH_3 protons and (b) hexane CH_2 and CH_3 protons as a function of temperature in the range from 0-60°C. Adapted with permission from [34]. Copyright (2020) American Chemical Society.

5. CSC-temperature of ethanol-hexane mixed solution

The Δδ values for individual protons of ethanol and hexane changed linearly to the higher field in the range from 0 to 60°C as shown in **Figure 2a** and **b**. Δδ for the OH proton changed 0.9 ppm during the temperature increase from 0 to 60°C, while those for CH_2 and CH_3 changed 0.1 ppm during the temperature increase from 0 to 60°C. Thus, the CSC-temperature under microwave irradiation was accurately determined using these relations for individual protons of a sample solution.

6. Microwave heating process of ethanol, hexane, and ethanol-hexane mixed solution

The microwave heating processes of ethanol were measured by plotting the CSC-temperature increase as a function of the microwave irradiation time, as shown in **Figure 3A(a)**. The temperature was initially set at 0°C, and the samples were continuously irradiated with 135 W (output power of microwave generator) microwave, during which NMR spectra were acquired every 30 s. The CSC-temperature of the CH_2 and CH_3 protons of ethanol increased from 0 to 30°C within 1 min and gradually increased to 58°C under microwave irradiation for 10 min. In contrast, the CSC-temperature of the OH protons increased from 0 to 35°C within 1 min and only slightly increased to 43°C for 10 min. The CSC-temperature of the OH protons deviated to a lower temperature than those of the CH_2 and CH_3 protons by 15°C under microwave irradiation for 10 min.

Figure 3A(b) shows the ^{1}H NMR spectrum of ethanol measured at 55°C (black) and that measured under microwave irradiation (135 W) for 10 min (orange) where the temperature was set at 0°C using the temperature controller of the NMR

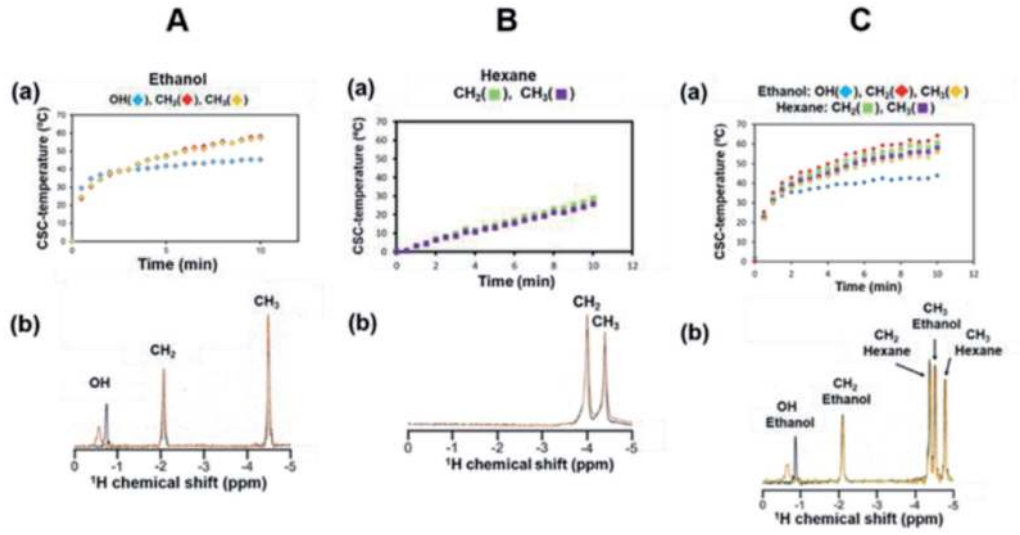

Figure 3.
A(a). CSC-temperatures as a function of microwave irradiation time. CSC-temperatures were determined using the slopes obtained for the individual protons. A(b). ^{1}H NMR spectrum for ethanol regulated at 55°C (black) and that under CW microwave irradiation for 10 min while controlling the instrument temperature setting at 0°C (orange). B(a). CSC-temperatures of CH_2 and CH_3 protons of hexane as a function of microwave irradiation time. B(b). ^{1}H NMR spectra of hexane regulated at 25°C (black) and that under CW microwave irradiation with the same condition as A(b) (orange). C(a). CSC-temperatures of CH_2, CH_3, and OH protons of ethanol and the CH_2 and CH_3 protons of hexane in ethanol-hexane (1:1, v/v) mixed solution as a function of microwave irradiation time. C(b). ^{1}H NMR spectra of ethanol-hexane (1:1, v/v) mixed solution regulated at 55°C (black) and that under CW microwave irradiation with the same condition as A(b) (orange). Adapted with permission from [34]. Copyright (2020) American Chemical Society.

spectrometer. The signal for OH protons under microwave irradiation for 10 min appeared 0.2 ppm lower field (orange). It is noted that the chemical shifts of the CH_2 and CH_3 protons completely overlapped with those measured at 55°C. Therefore, the ^1H chemical shifts of the CH_2 and CH_3 protons reflect the bulk temperature of the solution because CH_2 and CH_3 are non-polar groups. The lower field ^1H chemical shifts of OH protons under microwave irradiation are thus evidence of being induced by a non-thermal microwave effect in addition to the thermal microwave effect.

Figure 3B(a) shows the CSC-temperatures as a function of the microwave irradiation time. CSC-temperatures of the CH_2 and CH_3 protons of hexane increased gradually to 30°C under microwave irradiation for 10 min. A small temperature increase is attributed to the much lower dielectric loss factor of hexane than that of ethanol.

Figure 3B(b) shows ^1H NMR spectra of hexane at 30°C (black) and that after 10 min microwave heating (orange), where the black and orange peaks were completely overlapped.

Figure 3C(a) shows the CSC-temperature of the CH_2, CH_3, and OH protons of ethanol, and the CH_2 and CH_3 protons of hexane in ethanol-hexane (1:1, v/v) mixed solution. The CSC-temperature of the CH_2 and CH_3 protons increased to 40°C within 1 min and gradually increased to 55°C for 10 min. It is noted that all CH_2 and CH_3 protons increased in the same manner. On the other hand, the CSC-temperature of the OH proton was 15°C lower than those of the CH_2 and CH_3 protons.

Figure 3C(b) shows ^1H NMR spectra of the ethanol-hexane mixed solution at 55°C (black) and those after microwave heating for 10 min (orange), where the black and orange peaks were almost overlapped. On the other hand, the NMR peak of the OH proton under microwave irradiation appeared 0.2 ppm lower field, which indicates a 15°C lower temperature, as in the case of ethanol.

7. Microwave heating process of MBBA in the liquid crystalline state

Figure 4A shows the molecular structure of MBBA, which is known to form a liquid crystal phase below the liquid crystalline to isotropic phase transition temperature (Tc). **Figure 4B** shows the ^1H NMR spectrum of MBBA in the liquid crystalline state at 35°C, which is 5.5°C below the phase transition temperature (Tc = 40.5°C). A broad ^1H NMR spectrum with a 20 kHz linewidth was obtained for the liquid crystalline sample due to residual ^1H-^1H dipolar couplings. MBBA molecules tend to align along the magnetic field in the liquid crystalline phase; therefore, residual ^1H-^1H dipolar interactions induce a number of transitions with various degrees of dipolar interactions and this generates a significant line broadening. These dipolar interactions can provide insight into the order parameter of liquid crystals. **Figure 4C** shows a high-resolution ^1H NMR spectrum of MBBA in the isotropic phase that was obtained at 45°C, in which the narrow proton signals are well resolved, which enabled the assignment of the signals to their respective protons in the molecules [33].

The MBBA temperature was significantly increased by 5.0°C steps from 20.0°C below Tc to 40.5°C. As shown in **Figure 4D**, broad ^1H NMR signals of the liquid crystalline phase appeared alone at 35°C. At 40°C, the liquid crystalline phase had partly transitioned to the isotropic phase (**Figure 4D**). It was also evident that the liquid signals obtained at this temperature were broader than those of the fully isotropic phase, which may be attributed to the interaction of the isotropic and liquid crystalline phases, which induces a temperature distribution. This phase transition was completed at 40.5°C (**Figure 4D**), which indicates that the liquid crystalline and isotropic phases coexist near the phase transition temperature [33].

The temperature was then set at 20°C (20.5°C blow the Tc), followed by CW microwave irradiation at 130 W for 90 s, which generated weak isotropic phase

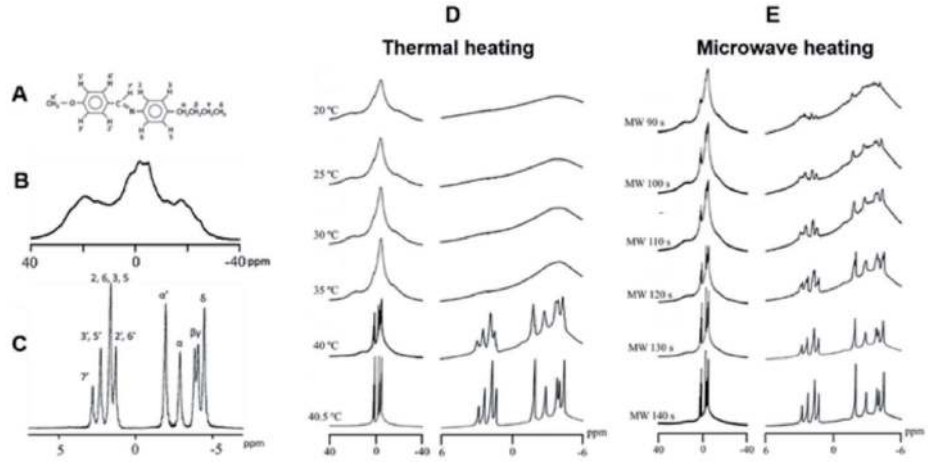

Figure 4.
A. Molecular structure of MBBA. B. ^{1}H NMR spectrum of MBBA in the liquid crystalline phase at 35°C. C. ^{1}H NMR spectrum of MBBA in the isotropic phase at 45°C, together with signal assignments for the individual protons. D. Series of ^{1}H NMR spectra of MBBA during the thermal heating processes. E. Series of ^{1}H NMR spectra during the microwave heating processes [33].

signals among the liquid crystalline phase signals (**Figure 4E**) even at a temperature lower than Tc. The temperature of the liquid crystalline phase was estimated to be 35°C from the assessment of the NMR linewidths with respect to the temperature. Such signals would not typically be expected until the temperature of the sample is close to its isotropic phase transition temperature of 40.5°C. This result indicates that microwave irradiation generated localized heating in the sample to form a small region of the higher temperature isotropic phase.

The temperature of the sample was successfully determined using *in situ* microwave irradiation NMR because the temperature of the MBBA liquid crystal was estimated with the NMR signal linewidth. It is noted that microwave irradiation generated a small fraction of the isotropic phase in the bulk liquid crystal at 35°C, even though this is 5.5°C lower than Tc (40.5°C). This result suggests non-equilibrium localized heating within the liquid crystalline sample [24].

8. Mechanism for microwave heating processes of liquid crystalline MBBA

The microwave-induced local heating phenomena observed in liquid crystalline MBBA is shown schematically in **Figure 5A**. Microwave irradiation generates a small amount of the isotropic phase inside the liquid crystalline sample below the phase transition temperature (Tc) (**Figure 5A(b)**). The dielectric loss for the isotropic phase is expected to be higher than that for the liquid crystalline phase, as shown in the MD simulation discussed in a later section. As a result, the isotropic phase is heated more efficiently by microwave irradiation, which induces a relatively higher temperature in the isotropic phase region. This phenomenon can be considered to be due to a type of non-equilibrium localized heating state, as observed in liquid–solid system [24]. The isotropic phase forms small particles and the surface of these particles interact with the surrounding liquid crystalline molecules to generate different linewidths than those produced by the bulk isotropic phase. This non-equilibrium heating state can be maintained over long time spans because the rate at which heat is obtained by the small isotropic phase particles by the absorption of microwave energy is balanced with the rate at which heat is dissipated to the bulk liquid crystalline phase. At a higher microwave power level,

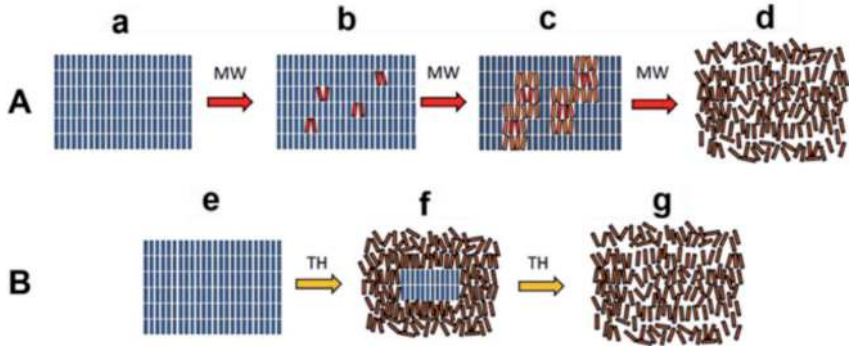

Figure 5.
A: Proposed (a, b, c and d) microwave (MW) heating processes within the liquid crystalline state. A small fraction of the liquid crystalline domain (hot spots) changes to the isotropic phase during microwave irradiation. The rate of temperature increase in this isotropic phase domain is higher than that in the liquid crystalline phase because of the larger dielectric loss for the isotropic phase. B: Schematic diagram showing the thermal heating process (e, f, and g) starting from the liquid crystalline phase to the isotropic phase [33].

the bulk isotropic phase increases (**Figure 5A(c)**), and eventually the entire sample transitions to the isotropic phase (**Figure 5A(d)**) [33].

In conventional thermal heating, the surface of the liquid crystalline state begins to melt to the isotropic state as shown in **Figure 5B(f)** and subsequently undergoes a rapid change to the isotropic state over the entire region of the sample (**Figure 5B(g)**).

9. CSC-temperature of MBBA in the isotropic phase

Figure 6A shows the structure of MBBA and the chemical shift values for individual protons as a function of temperature for isotropic phase MBBA. It is noted

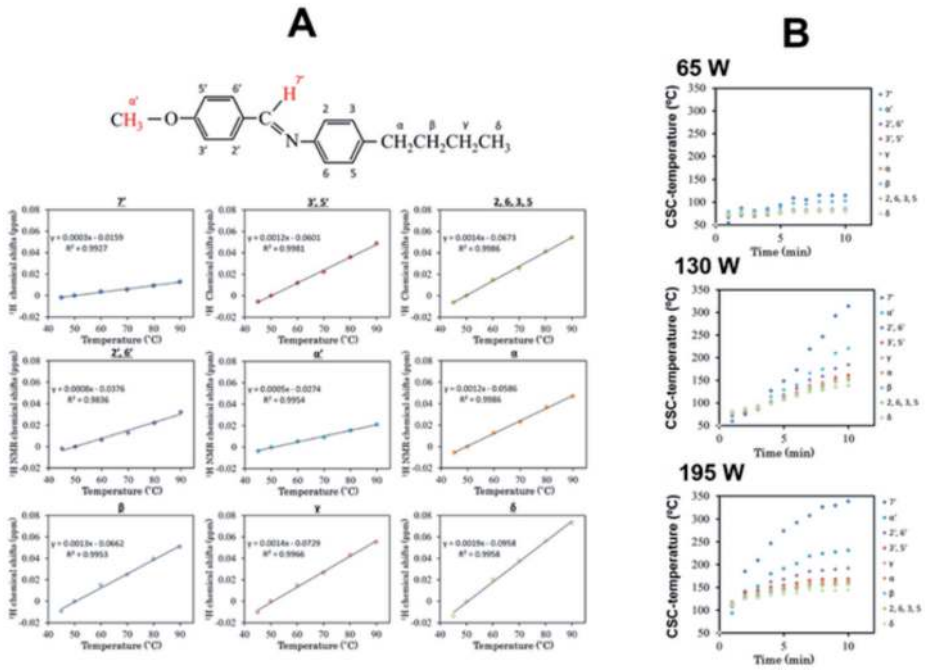

Figure 6.
A. Plots of ^{1}H chemical shift against setting the temperature of NMR spectrometer. B. Temperature as a function of the microwave irradiation time at a microwave power of 65, 130, and 195 W [33].

that the chemical shifts of different protons showed very different temperature variations. However, the chemical shift did exhibit a linear change as a function of the temperature for each different proton; therefore, it was possible to estimate the CSC-temperature of MBBA in the isotropic phase under microwave irradiation.

10. Microwave heating process of MBBA in the isotropic phase

Figure 6B presents an increase of the CSC-temperature for the MBBA sample under continuous wave (CW) microwave irradiation. The CSC-temperature increased from 50 to 70°C within 2 min under the application of 65 w CW microwave irradiation, based on the majority of protons. After microwave irradiation for 5 min, the CSC-temperature increase plateaued. However, there were significant variations in the CSC-temperatures among the protons; the 7′ and α' protons indicated 110 and 80°C, respectively. When microwave irradiation was applied at 130 W, the CSC-temperature was increased to 140°C for the majority of the protons, although values of 210 and 330°C were reached for the α' and 7′ protons, respectively. A further 8 min irradiation was required to obtain a saturated temperature. It is noted that the CSC-temperature of 7′ and α' protons showed higher CSC-temperature than the other protons. After microwave irradiation at 195 W, the CSC-temperature increased to 160°C within 5 min, although the α' and 7′ protons were discrepant from the other protons, with 220 and 350°C, respectively. Thus, α' and 7′ protons show much higher CSC-temperature than the other protons due to a non-thermal microwave effect as in the case of the OH protons of ethanol.

11. Characterization of non-thermal microwave effect of ethanol-hexane mixed solution and MBBA isotropic state

As shown in **Figure 3**, the CSC-temperature of the OH group of ethanol under microwave irradiation was considerably lower than those of the CH_2 and CH_3 protons. OH protons have a different CSC-temperature from the other protons. A temperature increase of the OH protons induces a higher field shift due to a reduction of hydrogen bonding under thermal heating [40]. Similar higher field shifts have been observed in H_2O protons [56]. In contrast, the CSC-temperatures of the OH protons are lower than the bulk temperature under microwave irradiation; therefore, the lower field shift of OH protons indicates the presence of a non-thermal microwave effect. On the other hand, the CSC-temperature of 7′ and α' protons of MBBA in the isotropic state showed much higher CSC-temperature than the other non-polar proton groups.

It is important to consider microwave heating from a physicochemical (thermodynamical) point of view to explain the energy flow mechanism. When energy is supplied to the solution under constant pressure (P) and temperature (T), the change of the Gibbs free energy (dG) is described as the difference of the changes in the enthalpy term dH = dU + d(PV), where dU is the change in the total internal energy which consist of dQ(heat) and dW(work), and entropy (TdS) terms. In the case of a solution state, the change of volume (V) is very small and the d(PV) term can be neglected, so that the Gibbs free energy is given by dG = dH – TdS = dQ + dW - TdS. In the case of a conventional thermal heating process, the change of the Gibbs free energy (dG) mainly increases the heat energy (dQ) term, which causes a temperature increase.

Figure 7 shows the energy flow processes from a physicochemical point of view. In the thermal heating process, the directions of polar molecules fluctuate

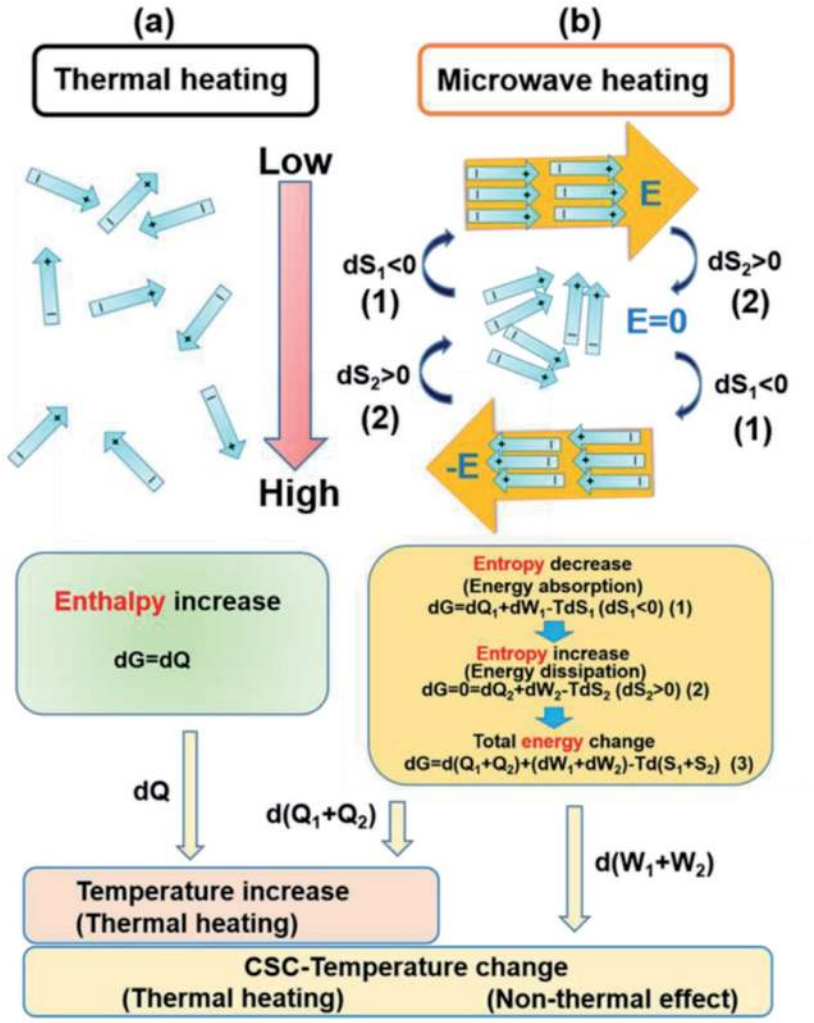

Figure 7.
Energy flow pathway under (a) conventional thermal heating and (b) microwave heating. Blue arrows indicate electric dipolar moment vectors and orange arrows indicate electric field vectors. Adapted with permission from [34]. Copyright (2020) American Chemical Society.

randomly, so that no net dipolar moment is induced (**Figure 7(a)**). In contrast, the microwave heating process induces order of the polar molecules to the electric field and a decrease of the entropy term ($dS_1 < 0$), therefore, the Gibbs free energy is increased to absorb microwave energy in the system as a first step, $dG = dQ_1 + dW_1 - TdS_1$, as shown in **Figure 7(b)**(1). The electric field oscillates with a frequency of 2.45 GHz; therefore, the polar molecular order is simultaneously reduced by an increase of the entropy term ($dS_2 > 0$) by conserving the Gibbs free energy, $0 = dQ_2 + dW_2 - TdS_2$, as a second step (**Figure 7(b)**(2)). Energy (TdS_2) thus dissipates as heat and work terms, $dQ_2 + dW_2$ to the system. By considering the sum of these two steps, $dG = d(Q_1 + Q_2) + d(W_1 + W_2) - Td(S_1 + S_2)$, (**Figure 7(b)**(3)), the heat term $d(Q_1 + Q_2)$ increases the temperature as thermal microwave effect and the work term $d(W_1 + W_2)$ may change the CSC-temperature for the OH group as a non-thermal microwave effect involving work terms such as molecular ordering and hydrogen bond formation. We interpret how the dW term changes the CSC-temperature of the OH groups in ethanol and H-C=N (7′) and CH_3-O (α') groups in MBBA.

It is important to note that polar molecules follow the oscillating electric field in a coherent manner. In this case, coherently aligned polar molecules are able to

interact with each other; therefore, there is an electrostatic interaction between the molecules that may specifically change the electric polarization in the polar group (OH, H-C=N, and CH_3-O groups) and thus cause a change of the electron density in these group, thereby inducing a chemical shift change. OH groups are polarized to O^-H^+ in the presence of an electric field, so that the electron density of OH protons may be reduced and the ^1H chemical shift is therefore expected to shift to the lower field under microwave irradiation. Since this process does not change the thermal heat energy of the system, the non-thermal microwave effect of dW is evident. In the case of ethanol, molecular order may increase the number of hydrogen bonds between the OH groups because ethanol molecules form clusters in a non-polar solvent [57], which induces a lower field chemical shift due to a microwave non-thermal effect that is in the direction opposite to conventional thermal heating. In summary, the entropy term is decreased to supply the microwave energy to the system and the entropy term is then subsequently increased because of dielectric loss by the change of electric field to dissipate the (dQ + dW) energy to the system (**Figure 7(b)**). As a result, the temperature is increased by the dQ term due to the thermal microwave effect, and the CSC-temperature of OH groups is further changed by the dW term due to the non-thermal microwave effect. MD simulation was further performed to characterize thermal and non-thermal microwave effects from a microscopic point of view in the following section.

12. Microscopic behavior of ethanol and MBBA molecules under microwave irradiation revealed by MD simulation

The microscopic behavior of ethanol in an ethanol-hexane mixed solution and MBBA molecules under microwave irradiation was further investigated using MD simulation. The results of ethanol-hexane and MBBA systems are shown in **Figure 8A(a–e)** and **B(f–h)**, respectively. Eight main simulations of the ethanol-hexane system were performed at 303, 313, 323, and 333 K in the presence and absence of an oscillating electric field. The net dipole moment induced by the oscillating electric field of 2.45 GHz is shown in **Figure 8(a)**. **Figure 8(b)** shows an ensemble of electric dipole moments along the x-direction (p_x) as a function of time at 303 K; p_x oscillated as a function of time. The phase of p_x was delayed from the electric field oscillation by a delay of around 36 ps, which was close to the experimentally measured average dielectric relaxation time of the ethanol-hexane mixture averaged around 30 ps [58]. This result is related to the dielectric constant and dielectric loss of the ethanol-hexane mixed solution, which induces the thermal microwave effect. Similar behavior was also observed in previous simulations of ice, water, and saline solutions [5]. In contrast, p_x fluctuated around zero in the absence of an electric field because of the random thermal fluctuation of the molecules in the solution.

The polar OH groups of ethanol molecules could affect the dipole moment of the system. Therefore, the orientation behavior of the OH groups was evaluated. The net direction of OH groups along the x-axis was calculated during all simulations, which is the sum of the length of all OH groups $\left(OH_x = \sum_i \left(H_{x,i} - O_{x,i}\right)\right)$. **Figure 8(c)** shows the net x-direction of OH groups during the simulations at 303 K in the presence (black) and absence (red) of the electric field E. The net direction oscillated as a function of time in the presence of an electric field, unlike the random fluctuation without an electric field. This indicates that microwave irradiation suppresses the random movement of the polar groups and causes their coherent alignment [59]. This alignment decreases the entropy of the system compare with

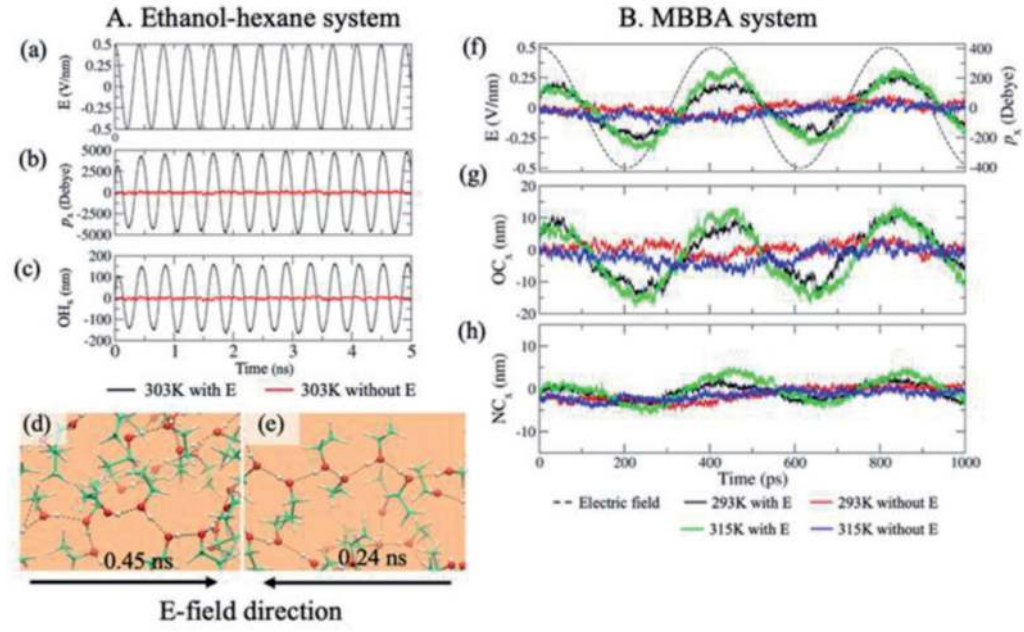

Figure 8.
A. Ethanol-hexane (1:1) system. (a) Applied electric field as a function of time. (b) the dipole moment of the simulations in the presence (black) and absence (red) of an electric field along the x-axis as a function of time at 303 K. (c) Net direction of OH groups as a function of time. (e) and (d) show examples of hydrogen bond formation in snapshots of the simulation at 0.24 and 0.45 ns under negative and positive electric field directions at 303 K, respectively. The hexane molecules were omitted for clarity. The dashed lines represent the hydrogen bonds between ethanol molecules, and the black arrows indicate the electric field directions in (d) and (e). Adapted with permission from [34]. Copyright (2020) American Chemical Society. B. MBBA system. (f) Applied electric field (dashed black) and the dipole moments of MBBA along the x-axis as a function of time. Net direction of C-O (g) and C=N (h) bonds of MBBA as a function of time. Black and green lines indicate the oscillation of these values as a function of time under the applied electric field at 293 and 315 K, respectively. Red and blue lines indicate the random fluctuations of the values without the electric field at 293 and 315 K, respectively.

that of the random orientations. **Figure 8(d)** and **(e)** show microscopic pictures of the ethanol molecules at 303 K in the presence of positive (+E) and negative (−E) electric fields at 0.45 and 0.24 ns, respectively. It is important to note that the orientation behavior of OH bonds along the electric field direction can be observed in these figures. In contrast, the directions of the OH groups were mostly oriented in random directions in the absence of an electric field [34]. Similar results were observed in other simulations at 313, 323, and 333 K (data are not shown). A time delay between the oscillation phases of the electric field and of the net OH direction was observed, which may have perturbed the ordered state of the polar groups and caused an increase in entropy due to the dielectric loss. The energy can consequently be dissipated into the system to increase the temperature via a thermal microwave effect. Furthermore, the OH groups formed a higher number of hydrogen bonds under the electric field compared to the groups without an electric field at higher temperatures [34]. This result explains the experimental data showing that the ^{1}H resonance of the OH group has a lower field shift and thus a lower CSC-temperature than the bulk temperature, as well as the lower field chemical shift increases at a higher temperature. It should be noted that this type of chemical shift induced by the electron polarization in the presence of an electric field under microwave irradiation may not appear under conventional thermal heating.

MD simulations of MBBA at 293 K (<Tc) and 315 (>Tc) K with and without the external electric field were also performed. **Figure 8(f)** shows the applied electric field (dashed black line) and the dipole moments of MBBA in these simulations

along the x-axis as a function of time. The black and green lines show the oscillation of the dipole moments along the x-axis under the applied electric field at 293 and 315 K, respectively. Due to the applied electric field, the dipole moment (black and green) at 293 and 315 K were delayed by around 32.5 and 18 ps, respectively. The values are close to the experimentally measured dielectric relaxation time of MBBA at 28 and 23.7 ps at 20 and 50°C, respectively [60]. In contrast, there is no oscillation of the dipole moment without the electric field at 293 K or 315 K, which indicates that the applied electric field affected the polar groups of the MBBA molecules.

The net direction of C-O and C=N groups of MBBA during these simulations were also analyzed, and are shown in **Figure 8(g)** and **(h)**, respectively. The α' and 7′ protons respectively bind to the C-O and C=N groups in the MBBA molecule, as shown in **Figure 6A**. **Figure 8(g)** and **(h)** show the net directions of the C-O and C=N groups as a function of time. The black and green lines show the net direction of C-O or C=N groups under the electric field at 293 and 315 K, respectively. The red and blue lines display the net directions in the simulations at 293 and 315 K without an electric field. The oscillation phase of the C-O groups is consistent with the phase of the dipole moments, as shown in **Figure 8(f)**, and their amplitudes are higher than those of the C=N groups shown in **Figure 8(h)**. This indicates that microwave heating has a more significant influence on the C-O groups of MBBA molecules.

These simulations showed the ordering of the polar molecules in the presence of an electric field as a non-thermal microwave effect. This polarization can only appear under microwave irradiation. Furthermore, this type of ordered state is also considered a low entropy state and is a distinct state occurring under microwave irradiation.

13. Microwave effects on chemical reaction processes

According to the MD simulations under microwave irradiation, the interactions between coherently ordered polar groups increased the number of hydrogen bonds in the ethanol-hexane mixed solution due to their coherent polarization (**Figures 7** and **8**). The formation of hydrogen bonds is due to the interaction between two OH groups, thus causing the energy of the work term to be supplied as a non-thermal microwave effect. This non-thermal microwave effect was experimentally verified by the observation of a lower field ^{1}H chemical shift of the OH protons in ethanol. This coherently ordered state of OH groups only appears under microwave irradiation and is different from the molecular order achieved by conventional thermal heating, even at the same bulk temperature of the system. In this microwave-induced ordered state, polar molecules are coherently aligned along with the alternately oscillated electric field. These coherently ordered molecules enable interaction between polar groups. Furthermore, the coherently ordered low entropy state may accelerate the chemical reaction rate between molecules with polar groups, as in the formation of hydrogen bonding in ethanol.

Similar to under microwave irradiation, polarizable molecules, or those with a dipole moment, will also gradually align with the direction of an oriented external electric field (OEEF). A sufficiently strong OEEF can completely orient a molecule or a molecular complex in space through interacting with its dipole and polarizability, thereby removing, in principle, the difficulty in orienting the molecules and the OEEF. Therefore, it is possible to enhance or control the chemical reactivity in catalysis by a decrease in the activation energy of the reaction [61, 62].

In the case of microwave irradiation, the electric field is oscillating at a frequency of 2.45 GHz. As discussed in the MD simulation and thermodynamics consideration, a polar molecule is coherently ordered along with the oscillating electric field. Unlike in the case of an applied OEEF, the coherent ordered state under microwave irradiation alternates at a frequency of 2.45 GHz. Nevertheless, the lifetime of a coherently ordered state is sufficiently long to accelerate the chemical reaction rate.

14. Conclusion

The CSC-temperatures of an ethanol-hexane mixed solution and MBBA in the isotropic state under microwave irradiation were accurately evaluated using the linear relationship of temperature with respect to the ^{1}H chemical shift changes ($\Delta\delta$) of individual protons. A CSC-temperature increase was observed as a function of the microwave irradiation time for CH_2 and CH_3 non-polar protons. The CSC-temperature for non-polar protons reflects the bulk temperature of the solution. A lowered CSC-temperature with lower field ^{1}H chemical shift was observed for OH polar protons than that with CH_2 and CH_3 non-polar protons in ethanol, and higher CSC-temperature was observed for H-C=N (7′) and CH_3-O (α') protons in MBBA. The lowered CSC-temperature of OH protons in ethanol under microwave irradiation which was lower than the bulk temperature is concluded to be the experimental evidence of a non-thermal microwave effect. In the microwave heating process, microwave energy is absorbed into the polar molecular system by the formation of an ordered state with lower entropy. Ordered dipolar molecules cannot completely follow the oscillating electric field; therefore, the ordered state becomes partly disordered, increasing the entropy. Microwave energy is simultaneously dissipated to the system as thermal and non-thermal microwave effects. These coherently ordered molecules interact strongly with each other to form hydrogen bonds between the OH groups of ethanol, and these interactions are considered to be due to a non-thermal microwave effect. MD simulation was carried out to confirm the theoretical validity of the experimentally observed increased lower field ^{1}H chemical shift, and the results were found to agree well. These non-thermal microwave effects play an important role in the intrinsic acceleration of chemical reaction rates between polar molecules under microwave irradiation. It is considered that the coherently ordered state reduces the activation energy for the reaction, which increases the reaction rate as catalysis.

Acknowledgements

This work was supported by KAKENHI Grant-in Aid (JP16H00756 to AN and JP20H05211 to IK) from the Ministry of Education, Culture, Sports, Science and Technology (MEXT), Japan and by KAKENHI Grant-in-Aid (JP15K06963 to AN and JP18H02387 to IK) from the Japan Society for the Promotion of Science (JSPS). The calculations were performed using clusters or supercomputers at the Research Center for Computational Science, Okazaki, Japan. The authors thank Ms. N. Yamaguchi for her financial support.

Author details

Akira Naito[1*], Yugo Tasei[1], Batsaikhan Mijiddorj[1,2], Izuru Kawamura[1] and Kazuyoshi Ueda[1]

1 Graduate School of Engineering, Yokohama National University, Yokohama, Japan

2 School of Engineering and Applied Sciences, National University of Mongolia, Ulanbaatar, Mongolia

*Address all correspondence to: naito@ynu.ac.jp

References

[1] Horikoshi S, Schiffmann RF, Fukushima J, Serpone N. Microwave chemical and materials processing. A Tutorial. Springer Nature. **2018**; 393 p. DOI:10.1007/978-981-10-6466-1

[2] Perreux L, Loupy A. A tentative rationalization of microwave effects in organic synthesis according to the reaction medium, and mechanistic considerations. Tetrahedron. **2001**;57:9199-9223. DOI: 10.1016/S0040-4020(01)00905-X

[3] Lidström P, Tierney J, Wathey B, Westman, J. Microwave assisted organic synthesis-a review. Tetrahedron. **2001**;57:9225-9283. DOI: 10.1016/S0040-4020(01)00906-1

[4] Kappe CO. Controlled microwave heating in modern organic synthesis. Angew. Chem. Int. Ed. **2004**;43:6250-6284. DOI: 10.1002/anie.200400655

[5] Tanaka M, Sato M. Microwave heating of water, ice, and saline solution: molecular dynamics study. J. Chem. Phys**. 2007**;126:034509. DOI:10.1063/1.2403870

[6] Kanno M, Nakamura K, Kanai E, Hoki K, Kono H, Tanaka M. Theoretical verification of nonthermal microwave effects on intramolecular reactions. J. Phys. Chem. A. **2012**;116:2177-2183. DOI: 10.1021/jp212460v

[7] Kappe CO, Pieber B, Dallinger, D. Microwave effect in organic synthesis: myth or reality? Angew. Chem. Int. Ed. **2013**;52:1088-1094. DOI:10.1002/anie.201204103

[8] Gedye R, Smith F, Westaway K, Ali H, Baldisera L, Laberge L, Rousell, J. The use of microwave ovens for rapid organic synthesis. Tetrahedron Lett. **1986**;*27*:279-282. DOI: 10.1016/S0040-4039(00)83996-8

[9] Giguere RJ, Bray TL, Duncan SM, Majetich G. Application of commercial microwave ovens to organic synthesis. Tetrahedron Lett. **1986**;29:4945-4948. DOI: 10.1016/S0040-4039(00)85103-5

[10] Adam D. Out of the kitchen. Nature. **2003**;421:571-572. DOI:10.1016/S0040-4039(00)85103-5

[11] Bogdal D, Lukasiewicz M.; Pielichowski J, Miciak A, Bednarz Sz. Microwave-assisted oxidation of alcohols using magtrieve. *Tetrahedron*. **2003**;*59*:649-653. DOI: 10.1016/S0040-4020(02)01533-8

[12] Yoshimura Y, Shimizu H, Hinou H, Nishimura S. A novel glycosylation concept; microwave-assisted acetal-exchange type glycosylations from methyl glycosides as donors. Tetrahedron Lett. **2005**;46:4701-4705. DOI:10.1016/j.tetlet.2005.05.046

[13] Parker M, Besson T, Lamare S, Legoy, M. Microwave radiation can increase the rate of enzyme-catalysed reactions in organic media. Tetrahedron Lett. **1996**;37:8383-8386. DOI: 10.1016/0040-4039(96)01544-4

[14] Shimizu H, Yoshimura Y, Hinou H, Hishimura, S. A new glycosylation method part 3: study of microwave effects at low temperatures to control reaction pathways and reduce byproducts. Tetrahedron. **2008**;64:10091-10096. DOI:10.1016/j.tet.2008.08.011

[15] Hoogenboom R, Wiesbrock F, Huang H, Leenen MAM, Thijs HML, van Nispen SFGM, van der Loop M, Fustin C, Jonas AM, Goby J, Schubert US. Microwave-assisted cationic ring-opening polymerization of 2-oxazolines: a powerful method for the synthesis of amphiphilic triblock copolymers. Macromelecules. **2006**;39:4719-4725. DOI: 10.1021/maq0609252a

[16] Iwamura T, Ashizawa K, Sakaguchi M. Efficient and echo-friendly anionic polymerization of acrylamide under microwave irradiation and hydrolysis of the obtained polymers by microwave irradiation. Macromolecules. **2009**;42:5001-5006. DOI: 10.1021/ma900769e

[17] Kajiwara Y, Nagai A, Chujo Y. Microwave-assisted synthesis of poly(2-hydroxyethyl methacrylate) (HEMA)/Silica hybrid using *in situ* polymerization method. Polymer J. **2009**;41:1080-1084. DOI: 10.1295/polymj.PJ2009157

[18] Yamada S, Takasu A, Takayama S, Kawamura K. Microwave-assisted solution polycondensation of L-lactic acid using a Dean-Stark apparatus for a non-thermal microwave polymerization effect induced by the electric field. Polym. Chem. **2014**;5:5283-5288. DOI: 10.1039/c4py00639a

[19] Pramanik BN, Mirza UA, Ing YH, Liu Y, Bartner PL, Weber PC, Bose AK. Microwave-enhanced enzyme reaction for protein mapping by mass spectroscopy: a new approach to protein digestion in minutes. Protein Sci. **2002**; *11*:2676-2687. DOI: 10.1110/ps.0213702

[20] Huang W, Xia, Y, Gao H, Fang Y, Wang Y, Fang Y. Enzymatic esterification between n-alcohol homologs and n-caprylic acid in non-aqueous medium under microwave irradiation. J. Mol. Cata. B Enzym. **2005**;*35*:113-116. DOI:10.1016j.molcatb.2005.06.004

[21] Lin, S, Wu C, Sun M, Sun, C, Ho Y. Microwave-assisted enzyme-catalyzed reaction in various solvent systems. J. Am. Soc. Mass Spectrom. **2005**;16:581-588. DOI: 10.1016/j.jasms.2005.01.012

[22] Herrero MA, Kremsner JM, Kappe CO. Nonthermal microwave effects revisited: on the importance of internal temperature monitoring and agitation in microwave chemistry. J. Org. Chem. **2008**;73:36-47. DOI: 10.1021/jo7022697

[23] Obermayer D, Gutmann B, Kappe CO. Microwave chemistry in silicon carbide reaction vials: separating thermal from nonthermal effects. Angew. Chem. Int. Ed. **2009**;48:8321-8324. DOI: 10.1002/anie.200904185

[24] Tsukahara Y, Higashi A, Yamauchi T, Nakamura T, Yasuda M, Baba A, Wada Y. In situ observation of nonequilibrium local heating as an origin of special effect of microwave on chemistry. J. Phys. Chem. C. **2010**;114:8965-8970. DOI:10.1021/jp100509h

[25] Naito A, Imanari M, Akasaka K. Separation of local magnetic fields of individual protons in nematic phase by state-correlated 2D NMR spectroscopy. J. Magn. Reson. **1991**;92:85-93. DOI: 10.1016/0022-2364(91)90249-S

[26] Naito A, Ramamoorthy A. Atomic-resolution Structural Studies of Liquid Crystalline Materials Using Solid State NMR Techniques. In: Ramamoorthy A , editor. Thermotropic Liquid Crystal: Recent Advances. Springer; **2007**;p.85-116. DOI: 10.1021/ja061153a

[27] Naito A, Imanari M, Akasaka K. State-correlated two-dimensional NMR spectroscopy: separation of local dipolar fields of protons in nematic phase of 4′-methoxybenzylidene-4-acetoxyaniline. J. Chem. Phys. **1996**;105:4502-4510. DOI: 10.1063/1.472300

[28] Akasaka K, Kimura M, Naito A, Kawahara H, Imanari M. Local order, conformation, and interaction in nematic 4-(n-pentyloxy)-4′-cyanobipheneyl and its one-to-one mixture with 1-(4′-cyanophenyl)-4-propylcyclohexane. A study by state-correlated 1H two-dimensional NMR spectroscopy. J. Phys. Chem.

1995;99:9523-9529. DOI: 10.1021/j100023a034

[29] Naito A, Tasei Y. Separation of local fields of individual protons in nematic phase of 4′-ethoxybenzylidene-4-n-butylaniline by microwave heating 2D NMR spectroscopy. *Mater. Sci. Technol. (M S&T)*. **2010**:2886-2894.

[30] Naito A, Makino Y, Tasei Y, Kawamura I. Photoirradiation and microwave irradiation NMR spectroscopy. In: The NMR Society of Japan, editor. Experimental approaches of NMR spectroscopy. Methodology and application of life science and materials science. Springer. **2018**;Ch 5: p. 135-170. DOI:10.1007/978-981-10-5966-7_5

[31] Akasaka K, Naito A, Imanari M. Novel method for NMR spectral correlation between the native and the denatured states of a protein. Application to ribonuclease A. J. Am. Chem. Soc. **1991**;113:4688-4689. DOI:10.1021/ja00012a052

[32] Tasei Y, Yamakami T, Kawamura I, Fujito T, Ushida K, Sato M, Naito A. Mechanism for microwave heating of 1-(4′-cyanophenyl)-4-propylcyclohexane characterized by *in situ* microwave irradiation NMR spectroscopy. J. Magn. Reson. **2015**;*254*:27-34.DOI: 10.1016/j.jmr.2015.02.002

[33] Tasei Y, Tanigawa F, Kawamura I, Fujito T, Sato M, Naito A. The microwave heating mechanism of N-(4-methoxybenzylliden)-4-butylaniline in liquid crystalline and isotropic phases as determined using *in situ* microwave irradiation NMR spectroscopy. Phys. Chem. Chem. Phys. **2015**;17:9082-9089. DOI: 10.1039/c5cp00476d

[34] Tasei Y, Mijiddorj B, Fujito T, Kawamura I, Ueda K, Naito A. Thermal and nonthermal microwave effects of ethanol and hexane mixed solution as revealed by in situ microwave irradiation nuclear magnetic resonance spectroscopy and molecular dynamics simulation. J. Phys. Chem. B. **2020**;147:9615-9624. DOI:10.1021/acs.jpcb,0c06383

[35] Caleman C, van der Spoel, D. Picosecond melting of ice by an infrared laser pulse: A simulation study. Angew. Chem. Int. Ed. **2008**;*47*:1417-1420. DOI:10.1002/anie.200703987

[36] Marklund EG, Ekeberg T, Moog M, Benesch JLP, Caleman C. Controlling protein orientation in vacuum using electric fields. J. Phys. Chem. Lett. **2017**;8:4540-4544. DOI: 10.1021/acs.jpclett.7b02005

[37] English NJ, MacElroy JMD. Molecular dynamics simulations of microwave heating of water. J. Chem. Phys. **2003**;118:1589-1592. DOI: 10.1063/1.1538595

[38] English NJ. Molecular dynamics simulations of microwave effects on water using different long-range electrostatics methodologies. Mol. Phys. **2006**;104:243-253. DOI: 10.1080/14733140500352322

[39] Garcia-Barnos B, Reinosa JJ, Penaranda-Fox FL, Fernandez JF, Catala-Civera JM. Temperature assessment of microwave-enhanced heating processes. Sci. Reps. **2019**;*9*:10809. DOI: 10.1038/s41598-019-47296-0

[40] Van Geet A. Calibration of the methanol and glycol nuclear magnetic resonance thermometers with a static thermistor probe. Anal. Chem. **1968**;40: 2227-2229. DOI: 10.1021/ac50158a064

[41] Van Geet AL. Calibration of methanol nuclear magnetic resonance thermometer at low temperature. Anal. Chem. **1970**;42:679-680. DOI:10.1021/ac60288a022

[42] Zuo CS, Metz KR, Sun Y, Sherry AD. NMR temperature measurements using a paramagnetic lanthanide complex. J. Magn. Reson. **1998**;133:53-60. DOI:10.1006/jmre.1998.1429

[43] Bielecki A, Burum DP. Temperature dependence of ^{207}Pb MAS spectra of solid lead nitrate. An accurate sensitive thermometer for variable-temperature MAS. J. Magn. Reson, Ser. A **1995**;116:215-220. DOI: 10.1006/jmra.1995.0010

[44] Hoffman RE, Becker ED. Temperature dependence of the ^{1}H chemical shift of tetramethylsilane in chloroform, methanol, and dimetylsulfoxide. J. Magn. Reson. **2005**;176:87-98. DOI: 10.1016/j.jmr.2005.05.015

[45] Abraham MJ, van der Spoel D. Lindahl E, Hess B. The GROMACS development team, GROMACS User Manual version 2018.7*, www.gromacs.org, 2019*.

[46] Huang J, MacKerell Jr AD. CHARMM36 all-atom additive protein force field: Validation based on comparison to NMR data. J. Comput. Chem. **2013**;34: 2135-2145. DOI: 10.1002/jcc.23354

[47] Vanommeslaeghe K, Hatcher E, Acharya C Kundu S, Zhong S, Shim J, Darian E, Guvench O, Lopes P, Vorobyov I, Mackerell Jr AD. CHARMM general force field: A force field for drug-like molecules compatible with the CHARMM all-atom additive biological force fields, J. Comput. Chem. **2010**;31:671-690. DOI: 10.1002/jcc.21367

[48] Harish Vagadia B, Vanga SK, Singh A, Raghavan V. Effects of thermal and electric fields on soybean trypsin inhibitor protein: A molecular modelling study. *Innov.* Food Sci. Emerg. Technol. **2016**;35:9-20. DOI:10.1016/j.ifset.2016.03.004

[49] Bussi G, Donadio D, Parrinello M. Canonical sampling through velocity rescaling. J. Chem. Phys. **2007**;*126*:014101. DOI: 10.1063/1.2408420

[50] Parrinello M, Rahman A. Polymorphic transitions in single crystals: A new molecular dynamics method. J. Appl. Phys. **1981**;52:7182-7190. DOI:10.1063/1.328693

[51] Darden T, York D, Pedersen L. Particle mesh Ewald: An N·log(N) method for Ewald sums in large systems. J. Chem. Phys. **1993**;98:10089-10092. DOI:10.1063/1.464397

[52] Essmann U, Perera L, Berkowitz ML, Darden T, Lee H, Pedersen LG. A smooth particle mesh Ewald method. J. Chem. Phys. **1995**;103:8577-8593.

[53] Hess B, Bekker H, Berendsen HJC, Fraaije JGEM. LINCS: A linear constraint solver for molecular simulations. J. Comput. Chem. **1997**;18:1463-1472. DOI: 10.1002/(SICI)1096-987X(199709)18:12<1463::AID-JCC4>3.0.CO;2-H

[54] Vaught A. Graphing with Gnuplot and Xmgr: Two graphing packages available under Linux. Linux J. **1996**;1996:7. DOI: 10.5555/326327.326334

[55] Humphrey W, Dalke A, Schulten K. VMD: Visual molecular dynamics. *J.* Mol. Graphics. **1996**;*14*:33-38. DOI: 10.1016/0263-7855(96)00018-5

[56] Dvinskikh SV, Yamamoto K, Dürr, UHN, Ramamoorthy A. Sensitivity and resolution enhancement in solid-state NMR spectroscopy of bicelles. J. Magn. Reson. **2007**;184:228-235. DOI: 10.1016/j.jmr.2006.10.004

[57] Sumi T, Dillert, R, Horikoshi S. Novel microwave thermodynamics

model for alcohol with clustering structure in nonpolar solution. J. Phys. Chem. B. **2015;**119:14479-14485. DOI: 10.1021/acs.jpcb.5b06168

[58] Utzel H, Stockhausen M. Dielectric Relaxation in Binary and Ternary Mixtures of Ethanol, Water, and Benzene or n-Hexane. Z. Naturforsch. **1985**;40a:588-595. DOI: 10.1515/zna-1985-0609

[59] Zhang Y–M, Li J-L, Wang J-P, Yang X-S, Shao W, Xiao S-Q, Wang -Z. Research on epoxy resin decomposition under microwave heating by using ReaxFF molecular dynamics simulations. RSC Adv. **2014**;*4*:17083-17090. DOI:10.1039/C4RA00473F

[60] Arora VP, Agarwal VK. Dielectric Relaxation Studies of N-(p-Methoxybenzylidene)-p-Butylaniline and N-(p-Ethoxybenzylidene)-p-Butylaniline in Benzene at Microwave Frequencies, J. Phys. Soc. Jpn. **1977**;42:908-910. DOI: 10.1143/JPSJ.42.908

[61] Shaik S, Ramanan R, Danovich D, Mandal D. Structure and Reactivity/Selectivity Control by Oriented-External Electric Fields. Chem. Soc. Rev. **2018**;14:5125-5145. DOI: 10.1039/C8CS00354H

[62] Shaik S, Danovich D, Joy J, Wang Z, Stuyver T. Electric-Field Mediated Chemistry: Uncovering and Exploiting the Potential of (Oriented) Electric Fields to Exert Chemical Catalysis and Reaction Control. J. Am. Chem. Soc. **2020**;142:12551-12562. DOI: 10.1021/jacs.0c05128